10. Knox, W. G., M. Hess, G. E. Jones, and H. B. Smith, *Chem. Eng. Progr.*, **57**, 66-71 (February, 1961).
11. Lange, N. A., "Handbook of Chemistry," 7 ed., Handbook Publishers, Sandusky, Ohio (1949).
12. Lippert, E. L., Jr., H. A. Palmer, and F. F. Blankenship, *Proc. Okla Acad. Sci.*, **31**, 115 (1950).
13. Miller, B., and E. R. Strong, *Am. Gas Ass'n. Monthly*, **28**, 63 (1946).
14. Palmer, H. A., Dissertation, Univ. Oklahoma, Norman, Oklahoma (1950).
15. Pieroen, A. P., *Rec. Trav. Chem.*, **74**, 995 (1955).
16. Sampson, J. E., Dissertation, Univ. Oklahoma, Norman, Oklahoma (1950).
17. Scheffer, F. E. C., and G. Meyer, *Proc. Acad. Sci. Amsterdam*, **21**, 1204-338 (1919).
18. Stackelberg, M. V., *Die Naturwissenschaften*, **36**, 327-33 (1949).
19. Stackelberg, M. V., and H. R. Muller, *Z. Elektrochemie*, **58**, 25-39, (1954).
20. Thompson, T. G., and K. H. Nelson, *Sears Foundation J. Marine Research*, **13**, 166-82 (1954), as quoted in *R and D Report No. 10*, p. 141, Office of Saline Water, U.S. Dept. of Interior, Washington, D. C. (1956).
21. Towlson, H. E., Thesis, Syracuse Univ., Syracuse, New York (1960).
22. Van der Waals, J. H., *Trans. Faraday Soc.*, **52**, 184 (1956).
23. ————, and J. C. Platteeuw, *Mol. Phys.*, **1**, 91 (1958).
24. ————, "Advances in Chemical Physics," Vol. 2, pp. 1-57, Interscience, New York (1959).
25. Weigandt, H. F., *Symposium of Nov. 1957*, Office of Saline Water, U.S. Dept. of Interior, Washington, D. C.
26. Williams, V. C., *U.S. Patent 2,947,-102* (March 7, 1961).
27. Williamson, K. D., Thesis, Univ. Oklahoma, Norman, Oklahoma (1950).

Manuscript received June 13, 1961; revision received September 19, 1961; paper accepted September 19, 1961. Paper presented at A.I.Ch.E. Lake Placid meeting.

Kinetics of the Catalytic Dehydration of Primary Alcohols

DONALD N. MILLER and ROBERT S. KIRK

University of Wisconsin, Madison, Wisconsin

The catalytic dehydrations of *n*-butanol, *n*-propanol, and ethanol to produce water and the respective olefins were studied for the temperature range 400° to 700°F. and over the pressure range 1 atm. to 100 lb./sq. in. gauge. Silica-alumina catalyst in bead form was used. Dehydration rates were found to be consistent with a single-site surface reaction-controlled mechanism on which was superimposed a mass transfer effect internal to the catalyst pellets. Rate constants for the three reactions are presented. The significances of their relative values and their temperature and pressure dependencies are discussed.

The apparent complexity of many heterogeneous reactions of commercial interest tends to encourage a reliance on empirical procedures in the design of reactors. Over the years basic information on gas-solid reaction kinetics has been steadily accumulating. Hopefully, with the continued growth of understanding in this field, more fundamental design procedures will be evolved and applied with confidence.

This study of a homologous series of alcohols undergoing analogous dehydration reactions over a silica-alumina catalyst illustrates a procedure of kinetic analysis from which useful design information can be obtained. There are some interesting possibilities for generalizing information of this type which the authors have tried to indicate. First, the same postulated mechanism and kinetics are shown to adequately describe all of the analogous systems. Secondly, the constants of the rate expression for the systems are shown to follow certain relationships that are at least qualitatively predictable.

Donald N. Miller is with E. I. du Pont de Nemours and Company, Wilmington, Delaware, and Robert S. Kirk is with California Research Corporation, La Habra, California.

EXPERIMENTAL

Reactor

A schematic flow diagram showing the reactor and other equipment used in this study is given in Figure 1. Additional detail may be found elsewhere (*10*). Alcohol forced in downflow through the reactor was preheated and vaporized in the upper annulus. Following reaction in the catalyst space in the lower center of the tube, the product gases passed through a quencher and then through an ice water-cooled condenser external to the reactor. The Duronze blocks were wrapped with heating wire and encased in transite pipe, the annulus between pipe and blocks being filled with rock wool insulation.

Equipment and Controls

Alcohol was fed to the reactor by displacing it from a feed tank with nitrogen. Rate of feed was measured in a rotameter ahead of the reactor and controlled by manually adjusting a needle valve at the rotameter inlet. Feed rates were high enough on all runs that mass transfer between the bulk gas stream and catalyst surfaces was not rate limiting.

Temperature was measured with an iron-constantan thermocouple centrally located in the catalyst bed. Check temperature measurements were also made periodically at the bottom center of the catalyst bed and at the bottom of the bed close to the tube wall. These temperatures were never found to differ from the center bed measurement by more than 1°C. Variac-controlled power input to the reactor heating wire was used to adjust reactor temperatures.

A Bourdon type of gauge located upstream of the reactor was used to measure reactor pressure. At the flow rates used in this work there was no appreciable pressure drop through the reactor unit. Desired pressure levels were maintained in the reactor by manually setting a needle valve located at the reactor outlet.

Off-gases from the ice water-cooled condenser passed through a wet test meter into a gas sampling system. Unreacted alcohol along with any water or aldehyde produced in the reactor were removed from the gas stream by condensation.

A molecular weight determination was made on the off-gas on all experimental runs. These along with the wet test meter readings permitted calculation of the total weights of off-gas evolved during the runs. These figures with the weights of condensate collected were checked against the total alcohol feed figures. The material balance closures were all within 5%.

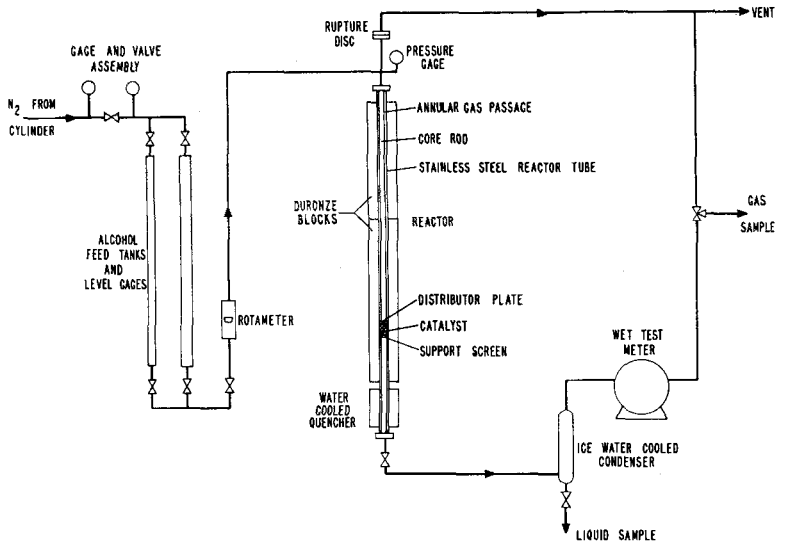

Fig. 1. Schematic of equipment.

Analyses

Electrometric Karl Fischer (*16*) analyses were made for water content in the condensed product on each run. Dehydration conversions were calculated based on the amount of this component formed.

Representative samples of the off-gas from various of the runs were checked qualitatively, by mass spectrograph for olefin contents. Trace quantities of olefins of higher and lower carbon number than the primary dehydration products were found in all cases.

Only one primary olefinic dehydration product is possible in the cases of both ethanol and *n*-propanol. Four isomers of the primary olefin are possible in the dehydration of *n*-butanol: 1-butene, cis and trans 2-butene, and iso-butene. The existence of all four forms over alumina and silica-alumina catalysts is reported in the literature (*1, 2, 3, 4, 15*). In this work the authors have restricted their attention to the study of over-all dehydration effects. No analyses were made to determine the isomeric product distributions.

Certain of the liquid samples were analyzed for aldehyde to determine the extent of dehydrogenation. This was done by gravimetrically measuring the amount of product formed by reacting aldehyde with 2, 4-dinitrophenyl hydrazine (*11*). The dehydrogenation conversions ran less than 5% of the corresponding dehydration conversions.

A mass spectrograph check of the liquid product showed no evidence of ether formation. Dehydration to ethers is reported in the literature as a side reaction over alumina catalyst (*1, 2, 3, 4*). This does not seem to occur to any appreciable extent over silica-alumina catalyst, however (*15*).

Feed Stock

Feed alcohols used and their specifications are given below:

Ethanol—99.9% purity by volume
n-Propanol—boiling range 96° to 98°C.
n-Butanol—boiling range 116° to 118°C.

All feed batches were treated with drierite and distilled to reduce the water contents below 0.2%. A correction for initial water content was made in computing dehydration conversions on all runs.

Run Procedure

Preliminary work showed that catalyst regeneration with steam and air mixtures could not be expected to give reproducible levels of catalyst activity. It was found however that the slight decrease in activity of fresh catalyst with time of exposure was linear and that neither heating or cooling affected this relationship appreciably provided the original temperature level was regained.

A single charge of catalyst was therefore used for a series of twenty to twenty-five runs with no regeneration. This catalyst was then replaced with a fresh charge for another series of runs. To check for slight differences in activity between charges of fresh catalyst the first few runs of each series were made with *n*-butanol at the reference conditions: 600°F., 1 atm. pressure, and W/F = 1.20 lb. catalyst hr./lb.-mole feed. To follow the decrease in activity with time of exposure every other subsequent run was made at some common or control temperature, pressure, and W/F. These latter conditions did not necessarily correspond to the reference conditions noted above.

Figure 2 shows a typical plot of dehydration conversions vs. exposure times for one series of runs. The control runs in this case were made with *n*-butanol at 500°F., 1 atm. pressure, and W/F = 1.20 lb. catalyst hr./lb.-mole feed. The drop in conversion in going from the reference to control conditions on Figure 2 reflects the change in temperature from 600° to 500°F.

For consistency all conversions were corrected to zero catalyst exposure time by a linear extrapolation parallel to a line drawn through the control conversions. The slope of the line through the control conversions represents the rate at which catalyst activity deteriorated in a given run series. Only slight differences were found in this activity decay characteristic between catalyst charges. The correction of conversions to zero catalyst exposure time reduced all conversions in a given run series to a common basis. Also any inaccuracies that might have arisen between catalyst charges from differences in the activity decay characteristic were minimized.

A final adjustment was made to the zero exposure conversions to reduce all values to a common initial catalyst activity. The first few runs of each series made at the reference conditions established the level of catalyst activity for that particular catalyst charge.

Each run lasted for 15 min., the first 5 min. being allowed for the attainment of a steady state condition after a change in variables. Checks made early in the experimental work showed 5 min. to be more than adequate to reach steady state. Data and samples were taken over the remaining 10-min. interval.

Dehydration conversions due to homogeneous, noncatalyzed reaction were checked at representative conditions by running the reactor with glass beads rather than catalyst in the reaction zone. These values were all small, in no case exceeding 10% of the total dehydration conversions. The latter were however corrected for the homogeneous conversions.

For each alcohol studied, ethanol, *n*-propanol, and *n*-butanol, dehydration con-

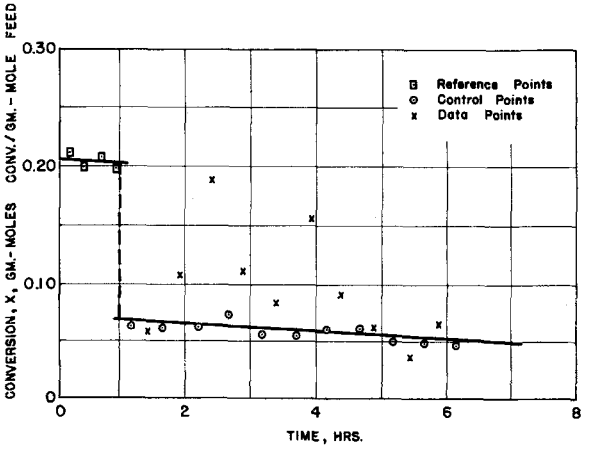

Fig. 2. Run series 147-168. Conversion vs. catalyst exposure time.

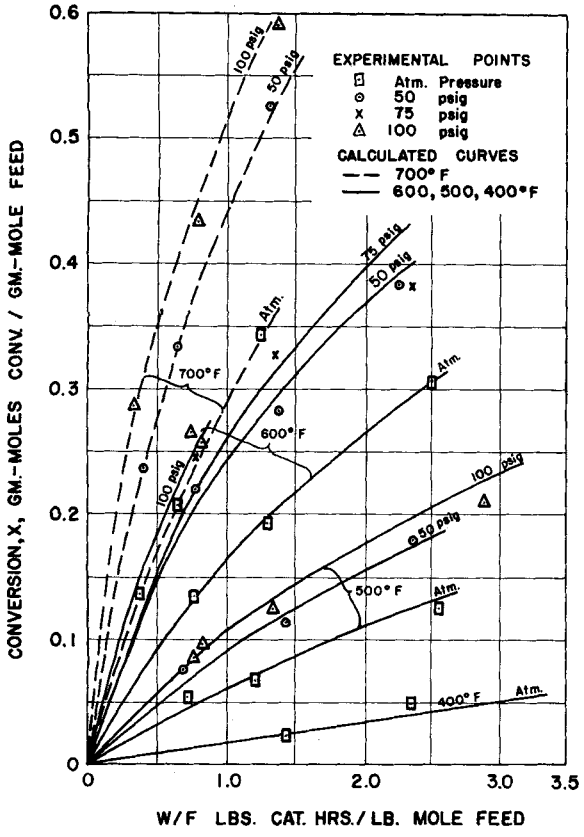

Fig. 3. *n*-Butanol. Conversion vs. W/F over −4+6 mesh catalyst.

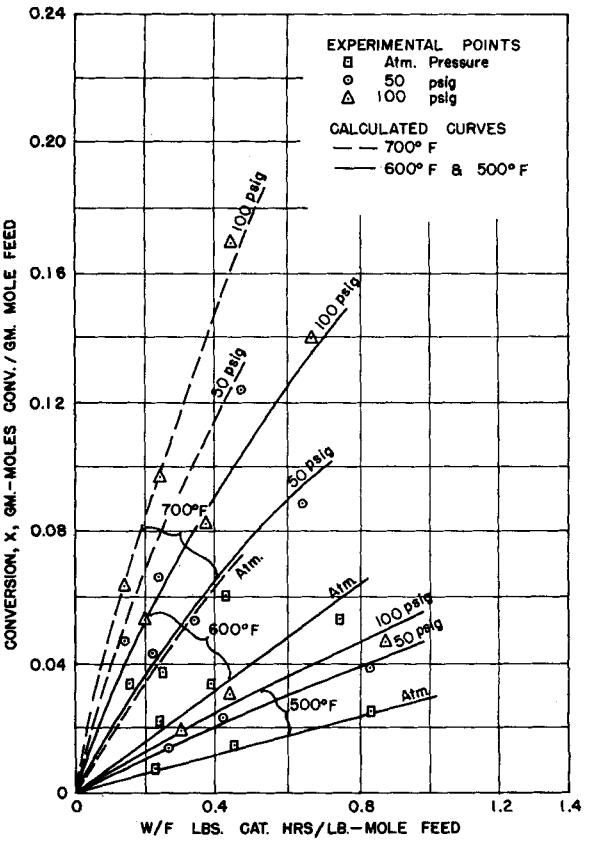

Fig. 5. Ethanol. Conversion vs. W/F over −4+6 mesh catalyst.

versions were obtained over 4- to 6-mesh catalyst for at least three pressures at each of three temperature levels. For each condition of pressure and temperature three different W/F values were used. These experimental points are

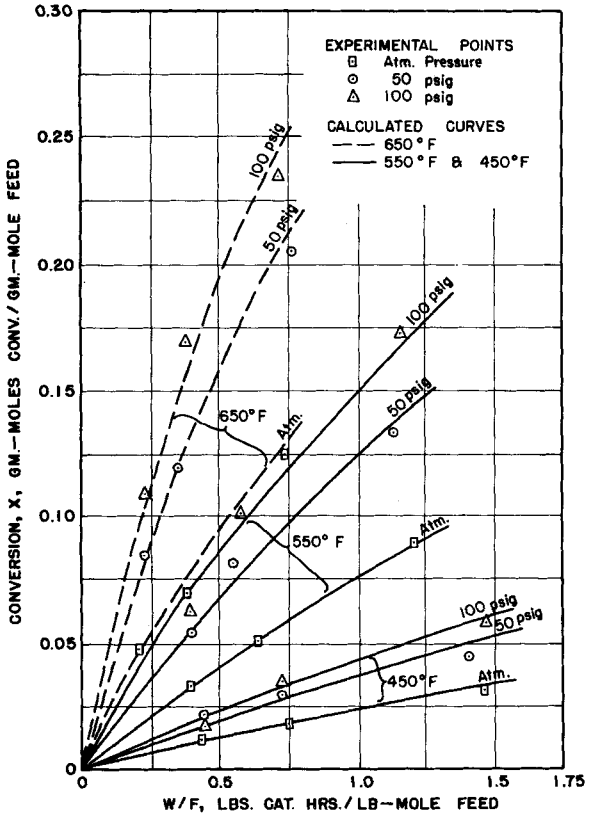

Fig. 4. *n*-Propanol. Conversion vs. W/F over −4+6 mesh catalyst.

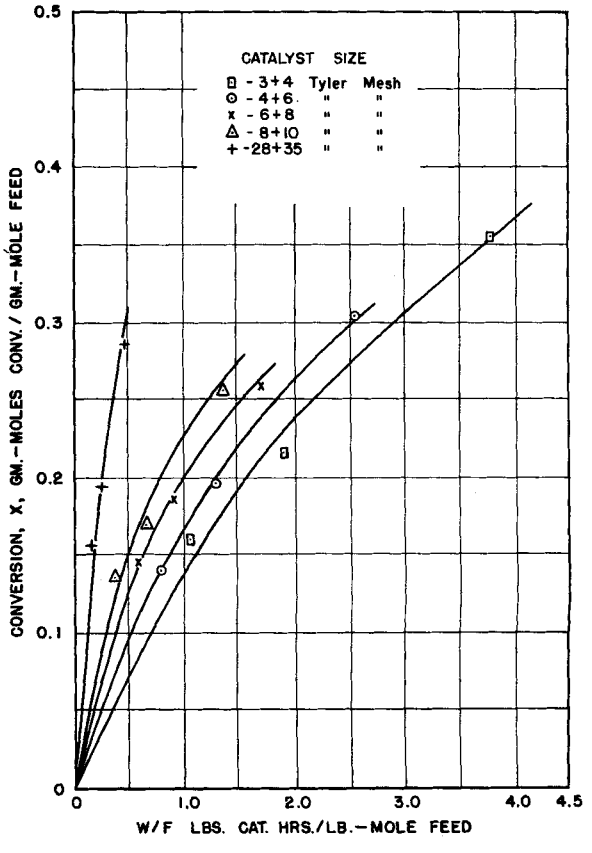

Fig. 6. *n*-Butanol. Conversion vs. W/F at atmospheric pressure and 600°F.

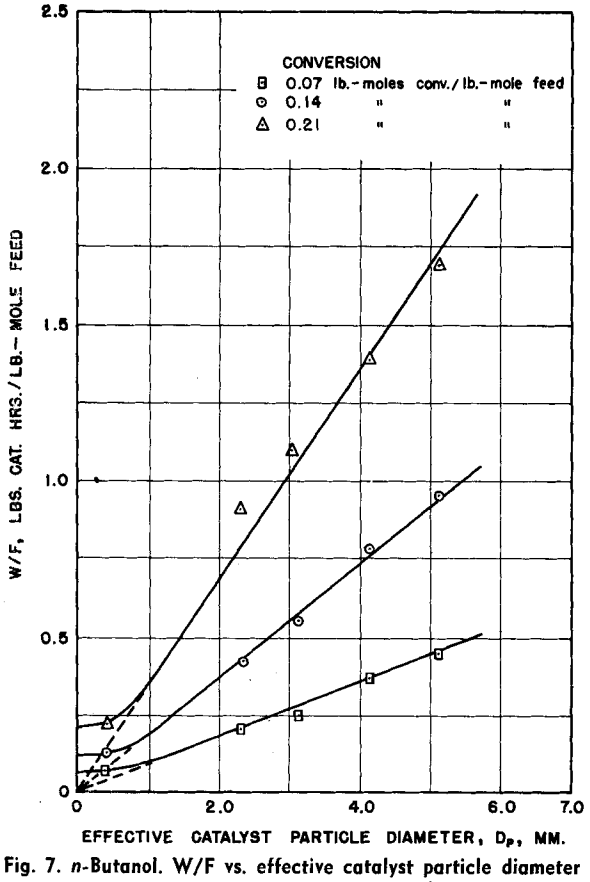

Fig. 7. *n*-Butanol. W/F vs. effective catalyst particle diameter at atmospheric pressure and 600°F.

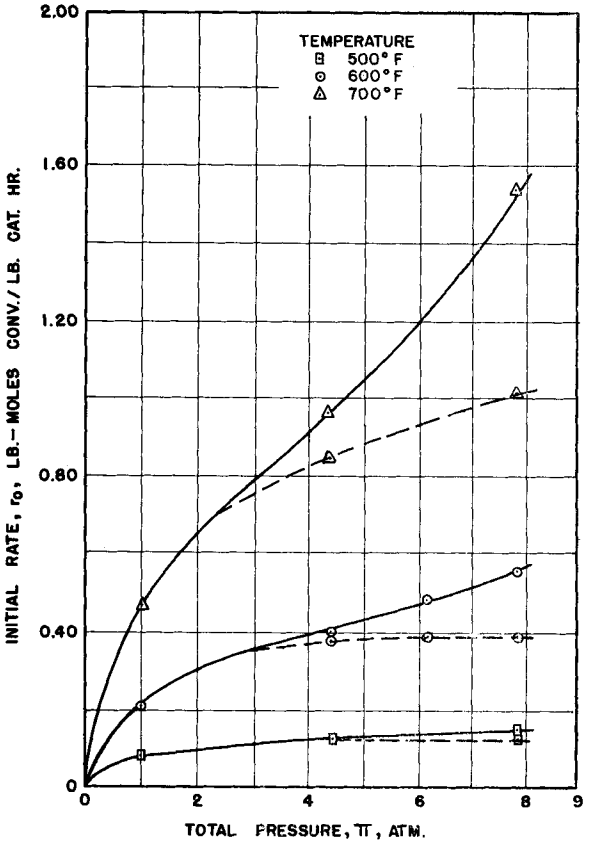

Fig. 8. *n*-Butanol. Initial rate vs. total pressure for −4+6 mesh catalyst.

shown plotted on Figures 3, 4, and 5.* The curves shown represent the calculated fit based on the kinetic analysis which follows.

In addition for each alcohol dehydration conversions were also obtained at atmospheric pressure and three different temperature levels over each of the following catalyst size ranges: 3 to 4, 6 to 8, 8 to 10, and 28 to 35 mesh.* This phase of the work was undertaken to measure catalyst effectiveness factors at atmospheric pressure. A typical set of conversion curves for the various catalyst sizes is given in Figure 6.

Catalyst

White TCC silica-alumina catalyst was used in this work. The catalyst received was screened into 3- to 4-, 4- to 6-, 6- to 8-, and 8- to 10-mesh fractions, and the fractions were then carefully picked over to remove any imperfect or discolored pellets. A 28- to 35-mesh fraction was made by breaking a portion of the 4- to 6-mesh fraction. Hammerlike blows rather than attrition were used in an effort not to alter or damage the active sites.

The total surface area for this catalyst reported by Socony (*12*) is 350 sq. m./g. Particle densities are roughly 1.15 g./cc., solid densities are about 2.30, and the internal void fraction is about 0.50. The mean pore radius, calculated from this information, is 25 Å. Mean effective particle diameters measured by the microscopic photographic technique described by Heywood (*9*) for the five size ranges are 5.11, 4.06, 3.05, 2.30, and 0.40 mm., respectively.

Effectiveness Factors at Atmospheric Pressure

On Figure 7 is shown a cross plot of the conversion data of Figure 6. Here W/F is plotted vs. effective particle diameter with conversion as the parameter. Three conversion values have been chosen which span the range of data taken. The curves are linear for the larger catalyst sizes and bend off to asymptotic values of W/F at small catalyst sizes. This behavior is consistent with the theoretical development of Thiele (*18*). The extrapolated W/F intercept at $D_p = 0$ represents condition $E = 1.0$.

Table 1. Catalyst Effectiveness Factors at Atmospheric Pressure

Catalyst size range, (Tyler mesh)	Temperature, (°F.)	Effectiveness factor
−3 + 4	500	0.15
	600	0.12
	700	0.10
−4 + 6	500	0.19
	600	0.15
	700	0.13
−6 + 8	500	0.24
	600	0.21
	700	0.16
−8 + 10	500	0.32
	600	0.27
	700	0.23
−28 + 35	500	0.98
	600	0.92
	700	0.90

Experimental effectiveness factors were obtained by making use of the inverse proportionality of E with W/F at constant conversion. This was done by dividing W/F at $D_p = 0$ by the appropriate W/F corresponding to the catalyst size of interest. These effectiveness factors were calculated at each of the three conversion levels and the results averaged. No difference was found in the effectiveness factors of the three alcohols. The experimental values are given in Table 1. They are shown plotted vs. absolute temperature in the top graph of Figure 12.

Averaging the effectiveness factors determined at the three conversion levels reduces the chances for errors in the extrapolations to $D_p = 0$. The close approach of these E values to a straight line Arrhenius relationship supports the fact that any such errors were minimized.

KINETIC ANALYSIS

Initial reaction rates were estimated by sketching curves through the experimental points shown on Figures 3, 4, and 5 and drawing lines tangent to these conversion curves at the origins. The initial rates were taken from the slopes of these tangent lines. These initial rates were then plotted vs. total pressure. A typical plot is shown in Figure 8.

* Complete tabular material has been deposited as document 7084 with the American Documentation Institute, Photoduplication Service, Library of Congress, Washington 25, D. C., and may be obtained for $1.25 for photoprints or for 35-mm. microfilm.

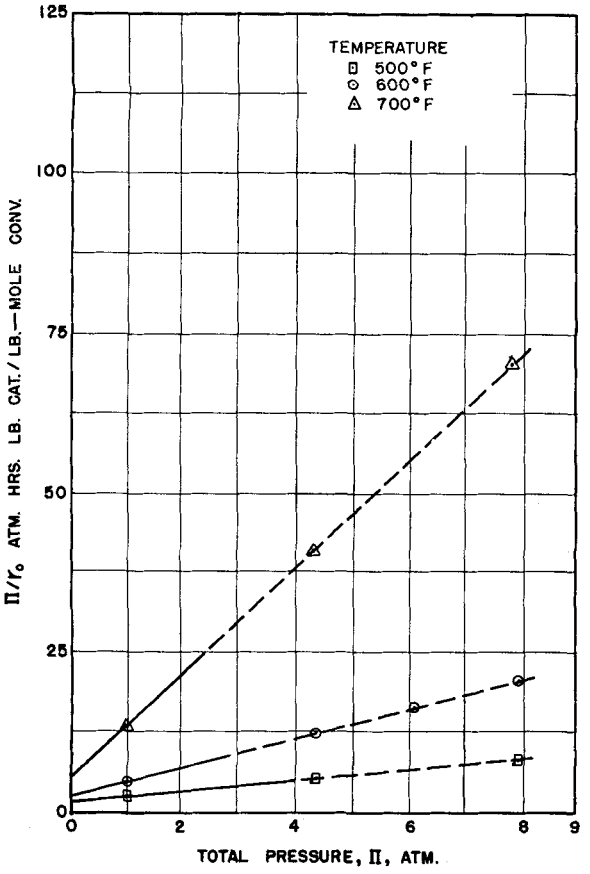

Fig. 9. *n*-Butanol. π/r_o vs. π for —4+6 mesh catalyst.

All of these curves show at lower pressures the downward concavity characteristic of a surface reaction rate-controlled mechanism. At higher pressures however initial rates go through an inflection or transition to an upward concavity. This becomes increasingly pronounced with increase in temperature. Such a transition could indicate a shift from one controlling mechanism to another, both being purely chemical in nature. What seems more probable however is that there is a change with pressure in the effectiveness of the heterogeneous system. All these considerations suggest the possibility of a basic surface reaction-controlled mechanism on which is superimposed the influence of a mass transfer effect internal to the catalyst pellets.

On this premise, on the assumption that the chemical element of the mechanism is single site and involves the sequence of steps listed below, a satisfactory fit was obtained to all the experimental data.

Steps in the Chemical Mechanism

1. Adsorption of alcohol.
2. Surface reaction involving the release of an olefin, water remaining adsorbed.
3. Desorption of water.

The surface reaction to be rate-controlling is presumed to be slower by order of magnitude than the adsorption and desorption steps.

A rate equation consistent with this mechanism can readily be derived (*8, 19*). This equation for the over-all alcohol dehydration

$$A \rightleftharpoons R + S \qquad (1)$$

follows:

$$r = \frac{EL\,k\,K_A\left(P_A - \frac{P_R P_S}{\nu}\right)}{1 + K_A P_A + K_R P_R} \qquad (2)$$

Expressed in terms of alcohol conversion x (moles of alcohol converted per mole of feed) rather than partial pressures, the rate expression can be written as in Equation (3):

$$r = \frac{EL\,k\,K_A\,\pi\left\{\left[\frac{1-x}{1+x}\right] - \left[\frac{x}{1+x}\right]^2\left[\frac{1}{(x^*)^2} - 1\right]\right\}}{1 + \left(\frac{1-x}{1+x}\right)K_A\,\pi + \left(\frac{x}{1+x}\right)K_R\pi} \qquad (3)$$

Substituting Equation (3) into the expression relating feed rate, reaction rate, catalyst quantity, and conversion

$$\frac{W}{F} = \int_o^x \frac{dx}{r} \qquad (4)^*$$

and integrating, one gets

$$\frac{W}{F} = \left\{\frac{1}{EL\,k\,K_A\,\pi} + \frac{1}{EL\,k}\right\}\left\{\left[\frac{x^*}{2} - \frac{(x^*)^3}{2}\right]\ln\frac{\left(1+\frac{x}{x^*}\right)}{\left(1-\frac{x}{x^*}\right)} + x(x^*)^2\right\} + \left\{\frac{2}{EL\,k\,K_A\,\pi} + \frac{K_R}{EL\,k\,K_A}\right\}\left\{\frac{(x^*)^2}{2}\ln\frac{1}{\left[1-\left(\frac{x}{x^*}\right)^2\right]} + \frac{(x^*)^3}{2}\ln\frac{\left(1+\frac{x}{x^*}\right)}{\left(1-\frac{x}{x^*}\right)} - x(x^*)^2\right\} \qquad (5)$$

Equation (2) can be simplified for initial rates in the experimental systems to

$$r_o = \frac{EL\,k\,K_A\pi}{1 + K_A\pi} \qquad (6)$$

Dividing through by total pressure and inverting one gets

$$\frac{\pi}{r_o} = \frac{\pi}{EL\,k} + \frac{1}{EL\,k\,K_A} \qquad (7)$$

* Equation (4) is applicable in catalytic systems where conditions approach steady state plug flow, constant temperature, and constant pressure.

Table 2. Rate Constants Summary

Alcohol feed	Temperature, (°F.)	$L\,k$, (lb.-moles conv./lb. cat. hr.)	K_A, (atm.$^{-1}$)	K_R, (atm.$^{-1}$)	K, (atm.)
n-Butanol	500	0.626	1.47	8.8	4,700
	600	2.96	0.867	4.8	9,500
	700	9.38	0.585	2.9	16,500
n-Propanol	450	0.226	1.19	12.6	1,200
	550	1.12	0.787	6.3	2,700
	650	4.41	0.579	3.7	5,300
Ethanol	500	0.466	0.525	8.8	100
	600	1.93	0.466	4.8	440
	700	4.66	0.413	2.9	1,000

π/r_o plotted vs. π gives a linear relationship with a slope of $(1)/(EL\,K)$ and an intercept of $(1)/(EL\,k\,K_A)$.

On Figure 9 are shown the π/r_o vs. π plots corresponding to the initial rate data in the lower pressure range of Figure 8. The dashed lines above 2 atm. on Figures 8 and 9 show how these relationships would look without the modifying mass transfer effect. From the slopes and intercepts of the π/r_o vs. π plots and with the effectiveness factors determined at atmospheric pressure, values of $L\,k$ and K_A were obtained for each alcohol at three temperatures. These values are given in Table 2 and are shown plotted vs. temperature in Figures 10 and 11.

Effectiveness factors for the higher pressures were obtained by factoring the effectiveness factors at atmospheric pressure in the ratio of experimental r_o (solid curves of Figure 8) to calculated r_o with no modifying mass transfer effect (dashed curves of Figure 8). These values are shown plotted vs. temperature in the lower two graphs of Figure 12.

Over-all equilibrium constants for the three dehydration reactions were calculated from free energy of formation data. Free energies of formation for the olefins and water were taken from Rossini (*14*); those for the alcohols were obtained through the Du Pont Company (*17*). These values are given in Table 2. They are high enough that equilibrium conversions in all cases closely approach unity.

For the condition $x^* = 1$, Equation (5) reduces to

$$\frac{W}{F} = \left\{ \frac{1}{EL\,k\,K_A\pi} + \frac{1}{EL\,k} \right\}$$

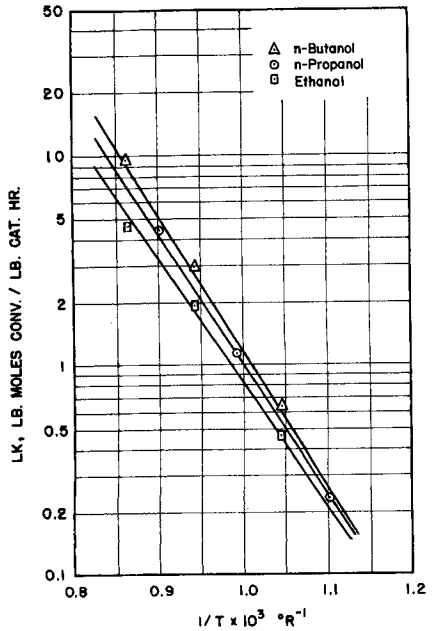

Fig. 10. *Lk* temperature relationship.

TABLE 3. SURFACE REACTION RATE CONSTANTS
$L\,K = LPZ \exp - E_a/RT$

Alcohol feed	Frequency factor $LPZ \times 10^{-6}$, (lb.-moles conv./ lb. cat. hr.)	Activation energy E_a, (k.-cal./g.-mole)	$\frac{[\Delta S‡ - \Delta S‡_{ET}]}{[\Delta S - \Delta S_{ET}]_{298.1(g)}}$	$\frac{E_a}{\Delta H_{298.1(g)}}$
n-Butanol	43.7	16.7	0.92	1.62
n-Propanol	23.4	16.2	0.83	1.98
Ethanol	9.34	15.4	—	2.23

$$x - \left\{ \frac{2}{EL\,k\,K_A\pi} + \frac{K_R}{EL\,k\,K_A} \right\} \{\ln(1-x) + x\} \qquad (8)$$

A plot of $\left\{ \frac{1}{EL\,k\,K_A\pi} + \frac{1}{EL\,k} \right\} x - \frac{W}{F}$ vs. $\{\ln(1-x) + x\}$ yields a straight line of slope $\left\{ \frac{2}{EL\,k\,K_A\pi} + \frac{K_R}{EL\,k\,K_A} \right\}$, thus providing a convenient means of evaluating K_R from the experimental data once the other constants are known. K_R values obtained in this way showed a considerable scatter. No differences in the K_R's for the three alcohols were apparent within the limits of experimental accuracy. Values obtained from the least-mean-squares fit to a K_R vs. temperature plot are given in Table 2.

With Equation (8) and the rate constants of Table 2, conversion vs. W/F curves were calculated and plotted on Figures 3, 4, and 5 to show the fit of the postulated mechanism to the experimental data points.

CONCLUSIONS

Surface Reaction Rate Constant

The following order of reactivity in the catalyzed dehydration is apparent by inspection of Figure 10:

ethanol < *n*-propanol < *n*-butanol

Table 3 shows the frequency factors and activation energies for the surface reaction rate constants. Both values appear to be approaching limits with increasing alkyl chain length. This is consistent with the inductive effect of the alkyl group. The electronegativity of this group increases, by diminishing increments, with increasing chain length, up to four or five carbons, where an asymptotic limit is closely approached.

Relative changes in activation entropy have been calculated from the relationship

$$\Delta S_1‡ - \Delta S_2‡ = R \ln \frac{(PZ)_1}{(PZ)_2} \qquad (9)$$

The ethanol dehydration values have been used as a common reference. It is interesting to note how closely the relative changes in activation entropy approach the corresponding relative changes in over-all entropy. The ratios of these numbers for the *n*-butanol and *n*-propanol dehydrations are given in Table 3.

Activation energies are roughly double the over-all heats of reaction. Ratios of these numbers are also given in Table 3. Changes in entropy and heats of reaction have been calculated from the data of standard references (*7, 13*).

Reactant Adsorption Constant

The K_A values also show the influence of the inductive effect of the alkyl group. With longer carbon chains the electron density at the oxygen atom of the alcohol is higher, and the tendency to adsorb at an acid silica-alumina site is therefore greater. The apparent approach to limiting K_A values with increasing chain length can be seen in Figure 11.

Product Adsorption Constant

K_R values showed the usual temperature dependency for equilibrium constants:

$$\ln K_R = \frac{\Delta S_R}{R} - \frac{\Delta H_R}{RT} \qquad (10)$$

A least-mean-squares fit to the experimental data gives the following characteristic ΔS_R and ΔH_R values:

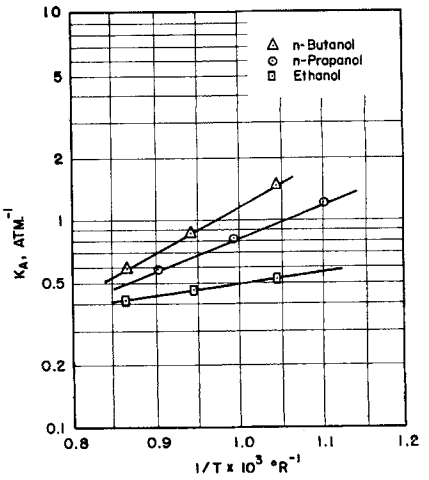

Fig. 11. K_A temperature relationship.

$\Delta S_R = -8.35$ cal./g.-mole °K.
$\Delta H_R = -6{,}760$ cal./g.-mole

The desorption step of the postulated mechanism is the same for the three dehydration reactions, involving in each case the detachment of a water molecule from an active catalyst site. The K_R's for the three alcohols would therefore be expected to be the same. No differences could be detected in the kinetic analysis.

Effectiveness Factor

Effectiveness factors were found to decrease with increasing temperature and to increase with increasing pressure. These relationships are shown on Figure 12. For a given catalyst the effectiveness factor is a function of the ratio of the reaction rate constant to effective diffusion coefficient, E tending to decrease with an increase in this ratio. A decrease in E with increase in temperature is to be expected, because reaction rate constants normally exhibit a stronger dependency on temperature than do diffusion coefficients.

The pressure dependency is less easily explained. Some of the increase in E with pressure can be attributed to the adsorption term in the denominator of the rate expression [see Equation (2)]. Any increase in total system pressure makes this term larger and thus decreases the effective rate constant. This effect is not great enough however to fully explain the magnitude of the change in E with pressure observed experimentally. Some of this change must be attributed to an increase in the effective diffusion coefficient with pressure.

As discussed by Wheeler (5), the ratio of the Knudsen to normal gas diffusion coefficient equals the ratio of pore diameter to mean free path of gas molecules. When this ratio is small, Knudsen type of diffusion is the rate-controlling, gas-phase mass transfer mechanism. These ratios, calculated for the experimental conditions of this study, covered the range 0.02 to 0.30. Normal gas diffusion seems not to have contributed strongly to the mass transfer process. On the other hand the Knudsen diffusion coefficient is pressure independent.

It is possible that a surface type of diffusion along the pore walls of the catalyst may have been the predominant mass transfer mechanism. Groves (6) has shown that in a system where there exists a strong tendency for molecules to adsorb, this type of mass transfer can overshadow the purely gas phase effects. Further, a surface diffusion coefficient, as pointed out by Groves, tends to increase with increase in pressure.

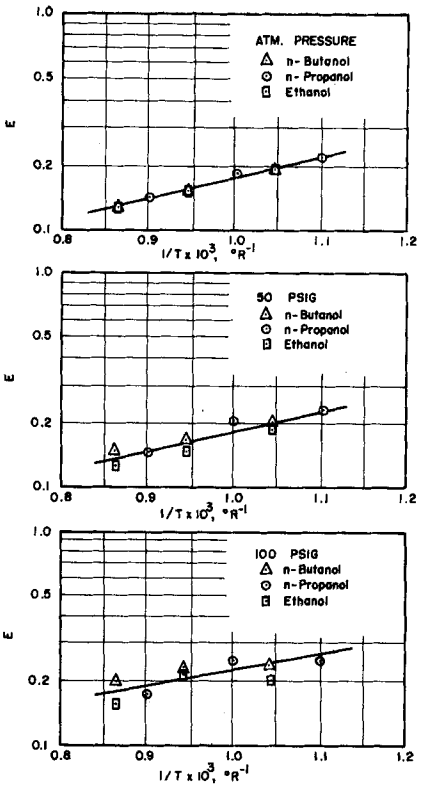

Fig. 12. Effectiveness factor temperature and pressure relationships.

ACKNOWLEDGMENT

The authors wish to express their appreciation to the Wisconsin Alumni Research Foundation and to the Eastman Kodak Company for the financial support given this project.

NOTATION

A = reactant
D_p = effective catalyst particle size, the diameter of a sphere having the same gross surface area as the particle
E = effectiveness factor
E_a = experimental activation energy
F = molal feed rate
$\Delta H_{298.1(g)}$ = change in enthalpy for a reaction at 298.1°K. with gaseous reactants and products
K = equilibrium constant
K_A = adsorption equilibrium constant for reactant A
K_R = adsorption equilibrium constant for product R
k = specific reaction rate constant
L = number of active sites per unit mass of catalyst
PZ = experimental frequency factor
P_A, P_R, P_S = partial pressures of component A, R, and S, respectively
R = gas constant
R = product
r = rate of conversion per unit mass of catalyst
r_o = initial rate of conversion per unit mass of catalyst
S = product
$\Delta S_{298.1(g)}$ = change in entropy for a reaction at 298.1°K. with gaseous reactants and products
$\Delta S^{\ddagger}$ = change of entropy in the formation of an activated complex
T = absolute temperature
W = mass of catalyst
x = moles conversion per mole of feed
x^* = equilibrium moles conversion per mole of feed
π = total pressure

Subscripts

ET = ethanol
1 = component
2 = component

LITERATURE CITED

1. Alvarado, A. M., *J. Am. Chem. Soc.*, **50**, 790 (1928).
2. Antipina, T. V., and A. V. Frost, *Zhur. Fiz. Khim.*, **24**, 860 (1960); *Chem. Abs.*, **45**, 937(d) (1951).
3. ————, *Vestnik Moskov Univ.*, **7**, 111 (1952); *Chem. Abs.*, **47**, 2026(a) (1953).
4. Balaceanu, J. C., and J. C. Jungers, *Bull. Soc. Chim. Belges*, **60**, 476 (1952); *Chem. Abs.*, **47**, 2683(b) (1953).
5. Emmett, P. H., ed., "Catalysis," Vol. 2, p. 126, Reinhold, New York (1955).
6. Groves, F. R., Ph.D. thesis, Univ. Wisconsin, Madison, Wisconsin (1954).
7. Hougen, O. A., and K. M. Watson, "Chemical Process Principles," Part II, pp. 701-708, Wiley, New York (1947).
8. *Ibid.*, Part III, pp. 917-926.
9. Heywood, H., *Proc. Inst. Mech. Engrs.*, **125**, 383 (1939).
10. Miller, D. N., Ph.D. thesis, Univ. Wisconsin, Madison, Wisconsin (1955).
11. Mitchell, J., Jr., ed., "Organic Analyses," Vol. 1, pp. 279-280, Interscience, New York (1953).
12. Nelson, T. W., Socony-Vacuum Oil Co., Inc., Letter to R. S. Kirk (June 10, 1954).
13. Perry, J. H., ed., "Chemical Engineers Handbook," 3 ed., pp. 236-243, McGraw-Hill, New York (1950).
14. Rossini, F. D., ed., "Selected Values of Properties of Hydrocarbons," National Bureau of Standards, Washington, D. C. (1947).
15. Sliepcevitch, C. M., and G. G. Brown, *Chem. Eng. Progr.*, **46**, No. 11, p. 556 (1950).
16. Smith, D. M., W. M. D. Bryant, and J. Mitchell, Jr., *J. Am. Chem. Soc.*, **61**, 2407 (1939).
17. Smith, D. M., E. I. du Pont de Nemours and Co., Letter to R. S. Kirk (April 20, 1955).
18. Thiele, E. W., *Ind. Eng. Chem.*, **31**, 916 (1939).
19. Yang, K. H., and O. A. Hougen, *Chem. Eng. Progr.*, **46**, 146 (1950).

Manuscript received March 8, 1961; revision received September 11, 1961; paper accepted September 13, 1961. Paper presented at A.I.Ch.E. Los Angeles meeting.